applied optics

Airborne ultraviolet imaging system for oil slick surveillance: oil–seawater contrast, imaging concept, signal-to-noise ratio, optical design, and optomechanical model

Zhenhua Shi,[1,2] Lei Yu,[1] Diansheng Cao,[1] Qingwen Wu,[1] Xiangyang Yu,[1] and Guanyu Lin[1,*]

[1]Changchun Institute of Optics, Fine Mechanics and Physics, Chinese Academy of Sciences, Changchun 130033, China
[2]University of Chinese Academy of Sciences, Beijing 100049, China
*Corresponding author: 1074124372@qq.com

Received 7 May 2015; revised 5 August 2015; accepted 7 August 2015; posted 7 August 2015 (Doc. ID 240216); published 27 August 2015

The airborne ultraviolet imaging system, which assesses oil slick areas better than visible and infrared optical systems, was designed to monitor and track oil slicks in coastal regions. A model was built to achieve the upwelling radiance distribution of oil-covered sea and clean seawater, based on the radiance transfer software. With this model, the oil–seawater contrast, which affects the detection of oil-covered coastal areas, was obtained. The oil–seawater contrast, fundamental imaging concept, analog calculation of SNR, optical design, and optomechanical configuration of the airborne ultraviolet imaging system are illustrated in this paper. The study of an airborne ultraviolet imaging system with F-number 3.4 and a 40° field of view (FOV) in near ultraviolet channel (0.32–0.38 μm) was illustrated and better imaging quality was achieved. The ground sample distance (GSD) is from 0.35 to 0.7 m with flight height ranges from 0.5 to 1 km. Comparisons of detailed characteristics of the airborne ultraviolet imaging system with the corresponding characteristics of previous ultraviolet systems were tabulated, and these comparisons showed that this system can achieve a wide FOV and a relative high SNR. A virtual mechanical prototype and tolerances analysis are illustrated in this paper to verify the performance of fabrication and assembly of the ultraviolet system.

OCIS codes: (040.7190) Ultraviolet; (280.4991) Passive remote sensing; (010.4450) Oceanic optics; (220.3620) Lens system design.

http://dx.doi.org/10.1364/AO.54.007648

1. INTRODUCTION

The coastal pollution of China, caused by accidental and illegal discharge of oil from ships and platforms, has heavily increased in the past decades and caused serious environmental problems. External accidents happen without control as the pollutants dumped into seawater are assumed from the controlled release by ships and oil production platforms, external accidents can never be controlled. Therefore, remote sensors are necessary in this field to monitor regions of oil slicks, together with artificial measurements to prevent the expansion of marine pollutions. Better performance is needed in spatial and temporal resolution for oil slick surveillance, which will enable the airborne remote sensor to be widely applied in coastal disaster observations. The cost and volume of the airborne remote sensor play a significant role in oil slick monitoring. Advanced sensors, such as laser fluorosensors, synthetic aperture radar (SAR), side-look airborne radar (SLAR), and passive microwave radiometry, are of high cost, are too large, and are hard to operate on a specialized aircraft. Thus, highly skilled operators are necessary [1,2]. In addition, certain adaptability limits of the advanced techniques become a concern when mapping the oil slick regions. For example, SAR cannot detect oil slicks when the wind speed is lower than 1.5 ms^{-1} or higher than 6 ms^{-1} [3]. Another challenge for SAR is the discrimination between oil slicks and look-alikes (e.g., phytoplankton). Furthermore, SAR imagery is expensive. When the rate of oil slick occurrence is extremely low, these sophisticated instruments on the airborne platform are not appropriate. Other optical sensors, such as ultraviolet, visible, and infrared sensors, are of low cost and whose installation and operation require no technical skills, while providing an inexpensive image.

Passive visible (approximately 0.4–0.7 μm) sensors are not capable of distinguishing oil slicks from the background as oil has no spectral characteristics in the visible band [4]. A darker shoreline may be mistaken for an oil slick in the visible channel. The infrared (primarily in the 8–14 μm wavelength region) sensor is inexpensive and commonly used for oil slick surveillance. However, the capability of these sensors on thickness

detection lies only between 20 and 70 μm, while the ultraviolet sensor can be applied to monitor oil film at thinner layers (down to 0.1 μm) [5]. Therefore, polluted areas with thinner oil films can be assessed successfully by an ultraviolet sensor, which is a remarkable characteristic in comparison with other optical sensors. Wagner *et al.* [6] presented standard infrared and ultraviolet sensor data and showed that the oil-covered areas estimated from the ultraviolet image differ by more than 50% from the areas acquired by the thermal infrared channel. The reason is that very thin films cannot be detected in the infrared channel. Thermal look-alike radiation (e.g., seaweed, shorelines, and ships) similar to the radiation from oil slicks may lead to a false result in the infrared channel. Catoe and Orthlieb [7] showed that the ultraviolet imagery of part of all four types of oils used in the Gulf of Mexico experiment are brighter than the water background, while the darker oil pollution areas surrounded by the brighter areas can also be identified from the background. Although sun glint [8] may result in a false detection for the ultraviolet sensor, the appropriate zenithal viewing angle and azimuthal angle from the Sun can decrease these unfavorable effects and improve the imaging quality of oil slicks in coastal areas. The ultraviolet sensor can also distinguish the shoreline, which is an interference source for visible and infrared sensors, from coastal areas in the case of misidentification between the oil-covered ocean and the coastline. In terms of the above aspects, such as larger detectable areas, higher oil–water contrast, and less look-alike radiation influence from the background, ultraviolet sensors are at a more obvious advantage than visible and infrared sensors. Timely and effective responses are important and necessary for monitoring oil slicks. Airborne optical systems, which have advantages of high spatial resolutions and short revisit periods, can be used for small- and mid-scale oil pollution. An ultraviolet imaging system aboard an airborne platform is a passive sensor since it uses reflected sunlight in the near ultraviolet regions (0.32–0.38 μm) for oil slick monitoring.

The airborne ultraviolet system can provide access to the available and relevant oil slick signatures. Previous generations of ultraviolet imaging systems provide a broad overview of oil pollution but do not have the necessary SNR and field of view (FOV). Some ultraviolet systems aboard aircrafts, such as the HU-25A aircraft [9], the DO 28 D2 surveillance aircraft [10], the new Cessna 402C aircraft [11], have a relatively low SNR. The SNR of the ultraviolet line scanner onboard the HU-25A aircraft is only 17 dB, while the new-style ultraviolet push-broom camera provides only a 15 deg FOV [12,13]. The capability of the new-style ultraviolet push-broom camera aboard airborne systems for oil slick monitoring was examined by Yin *et al.* [12,13]. They studied the marine oil slicks in the Yellow Sea area of China and showed that (a) the oil pollution detection is available through the near ultraviolet channel and (b) the images of the green and red bands show little difference between the oil slick areas and the background. Therefore, the near ultraviolet (0.32–0.38 μm) camera onboard the airborne platform can be applied to monitor oil pollution in coastal areas. The narrow FOV of the optical detection system would increase flight frequency, cost, and time for oil slick pollution surveillance. The push-broom camera with a relatively narrow FOV proposed by Yin would not be economical for detecting mid-scale oil slick pollution. The low signal returned from the oil-polluted areas of the ultraviolet camera would decrease imagery quality, and limited coverage of the ultraviolet camera would increase flight costs. Therefore, an ultraviolet imaging system with a wider FOV and a higher SNR was conceived in this paper for the mid- and small-scale oil slick monitoring.

2. SYSTEM CONSIDERATION

A. Oil–Seawater Contrast

Oil in the sea can be detected by optical remote sensors due to the oil–water contrast between the oil-covered ocean and the background ocean. Visibility of oil in seawater depends on the oil–seawater spectral contrast, which is defined as the difference in measured upwelling radiance between the oil-covered and ocean water [14,15]. The upwelling radiance $L_u(0^+;\lambda;\theta_v;\Delta\varphi)$ [16] is the sum of three main contributions: the atmospheric path radiance, the reflected sky radiance contribution $L_{\text{sky-refl}}(0^+;\lambda;\theta_v;\Delta\varphi)$, and the water-leaving radiance $L_{\text{wl}}(0^+;\lambda;\theta_v;\Delta\varphi)$. Generally, the atmospheric path radiance can be removed from the remote data. Thus, the upwelling radiance $L_u(0^+;\lambda;\theta_v;\Delta\varphi)$ can be expressed as

$$\begin{aligned} &L_u(0^+;\lambda;\theta_v,\Delta\varphi)\\ &\quad= L_{\text{sky-refl}}(0^+;\lambda;\theta_v,\Delta\varphi)+L_{\text{wl}}(0^+;\lambda;\theta_v,\Delta\varphi)\\ &\quad= r_w L_{\text{sky}}(0^+;\lambda;\theta_v,\Delta\varphi)+L_{\text{wl}}(0^+;\lambda;\theta_v,\Delta\varphi), \end{aligned} \tag{1}$$

where r_w is the reflectance of the air–seawater interface or the air–oil interface, $L_{\text{sky}}(0^+;\lambda;\theta_v;\Delta\varphi)$ is the diffuse skylight radiance, "0^+" means the upper interface of air–seawater or air–oil, λ is the wavelength, θ_v is the zenithal viewing angle, φ_v is the viewing direction relative to the Sun incidence plane, and $\Delta\varphi=\varphi_s-\varphi_v$ is the difference between the azimuthal viewing and solar incidence plane.

The oil–water contrast can be expressed as the following equation, with the overall theoretical assumptions and detailed derivation described in [7]:

$$C(0^+;\lambda;\theta_v,\Delta\varphi)=\frac{L_u^o(0^+;\lambda;\theta_v,\Delta\varphi)-L_u^w(0^+;\lambda;\theta_v,\Delta\varphi)}{L_u^w(0^+;\lambda;\theta_v,\Delta\varphi)}, \tag{2}$$

where $L_u^w(0^+;\lambda;\theta_v;\Delta\varphi)$ is the upwelling radiance from clean seawater and $L_u^o(0^+;\lambda;\theta_v;\Delta\varphi)$ is the upwelling radiance from oil-covered seawater.

The relationship between viewing geometry and Sun direction is shown in Fig. 1 [17]. θ_s is the solar zenith angle and we assume a solar azimuthal angle of $\varphi_s=0$, so $\Delta\varphi=-\varphi_v$. Therefore, the azimuthal viewing angle is positive when the azimuthal viewing plane rotates in the counterclockwise direction from the solar incidence plane.

The upwelling radiance is concerned with the reflectivity of the oil-covered sea surface and the sea surface. The dependence of the sea surface reflectance or oil reflectance, which is not an inherent optical property of the surface, on sky conditions, wind speed, solar zenith angle, and viewing geometry is known [18]. The target region reflectance r_w can be calculated and the detailed derivation process can be seen in [19]. However, the measured reflectance of the sea surface and diesel fuel in

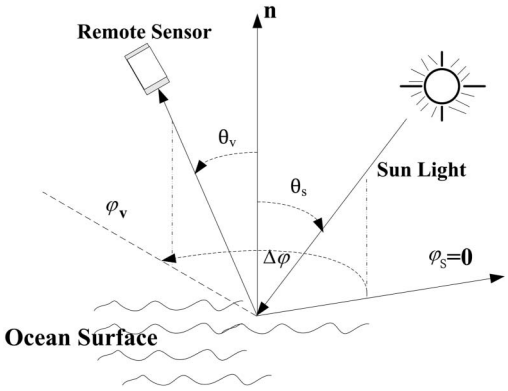

Fig. 1. Geometry positions of the remote sensor and Sun.

the seawater was applied to calculate the upwelling radiance, as the reflectance of the sea surface and diesel fuel in the seawater was different with different optical parameters. Fang *et al.* [20] sprinkled four kinds of oil slicks above clean seawater in the laboratory and acquired reflectivity of several kinds of classical oil slicks on seawater and clean seawater. The reflectance of diesel fuel and clean seawater is shown in Fig. 2. When the thickness of the oil is 400 μm, the reflectivity of almost all of the oil film measured in the laboratory is larger than clean water in the near ultraviolet region. The absolute value of the oil–seawater contrast means whether oil in seawater is detectable [21]. To simplify the oil–seawater model, it is assumed that the thickness of the oil slick is 400 μm. For the purpose of acquiring oil–seawater contrast, reflectivities of the oil-covered sea surface and ocean surface are necessary.

The minimum reflectivity of diesel fuel is about 0.085, as shown in Fig. 2. Tang [22] pointed out that there was still a controversy of reflectance of ocean surface in different sea conditions. Mobley suggested that the sea surface reflectance $r_w \approx 0.028$ is acceptable with wind speed less than 5 ms^{-1}, reasonable viewing geometry, and a clear sky. Although the reflectance of clean water is acquired in the laboratory [20], it was not applied to calculate the upwelling radiance in this paper, as the properties, such as sky condition, wind speed, and roughness of the ocean water, are different from that of clean water. Therefore, a sea surface reflectance of $r_w \approx 0.028$ is applied to calculate the upwelling radiance of the sea surface. Mobley [23] suggested that a viewing direction of $\theta_v = 40°$ from the nadir and $\varphi_v = 135°$ ($\Delta\varphi = -135°$) from the Sun can minimize the effects of sun glint and nonuniform sky radiance. Therefore, a model, which is applied to generate upwelling radiance as a function of wavelength in the remote sensor with a solar zenith angle of $\theta_s = 30°$, was established using MODTRAN software [24] according to the viewing geometry proposed by Mobley. The 1976 U.S. Standard Atmosphere profiles with an open-ocean marine aerosol profile in the boundary layer and no clouds and rain model were used for the calculation of radiance at a 1 km flight height. Other parameters of this model are defaults according to the MODTRAN default models and default values. From the above assumptions and requirements, the spectral upwelling radiance distribution with different wavelengths of clean seawater and diesel-fuel-covered ocean was simulated by MODTRAN software, as shown in Fig. 3.

Figure 4 shows the oil–seawater contrast obtained by Eq. (2) and the upwelling radiance distribution of seawater and diesel-covered sea in Fig. 3. As it shows, the diesel–water contrast varies from a value of 8% to 14.2% with a wavelength range of 0.32–0.38 μm. The oil spilled on seawater could be detected easily by an ultraviolet airborne remote sensor with relatively large spectral contrast. Integrated total radiance L_0 acquired by MODTRAN software is significant in calculating the SNR of the optical sensor at a height of 0.5–1 km above oil-polluted coastal areas.

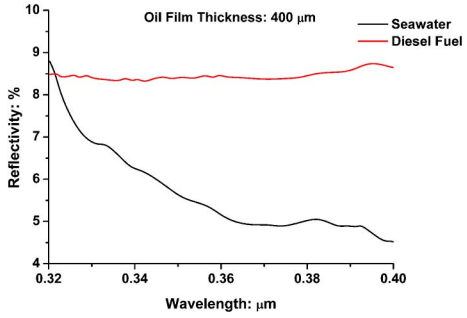

Fig. 2. Reflectivity of a calm, flat seawater surface and diesel fuel spilled on seawater under laboratory conditions with a viewing direction of $\theta_v = 40°$ from the nadir and a solar zenith angle of $\theta_s = 30°$ in a clear sky case in summer [20].

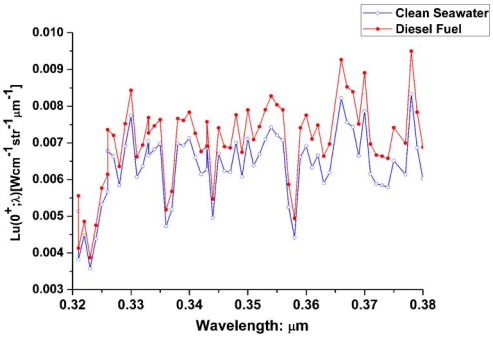

Fig. 3. Upwelling radiance distribution of seawater and diesel fuel spilled on seawater simulated by MODTRAN with the viewing direction of $\theta_v = 40°$, $\varphi_v = 135°$ and a light incidence angle of $\theta_s = 30°$.

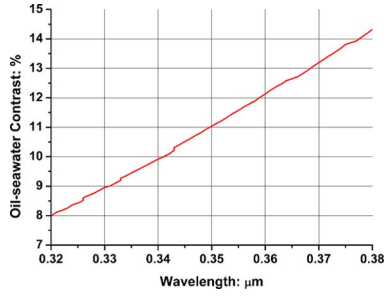

Fig. 4. Diesel–seawater spectral contrast as a function of wavelength, where the thickness of the diesel fuel film is 400 μm.

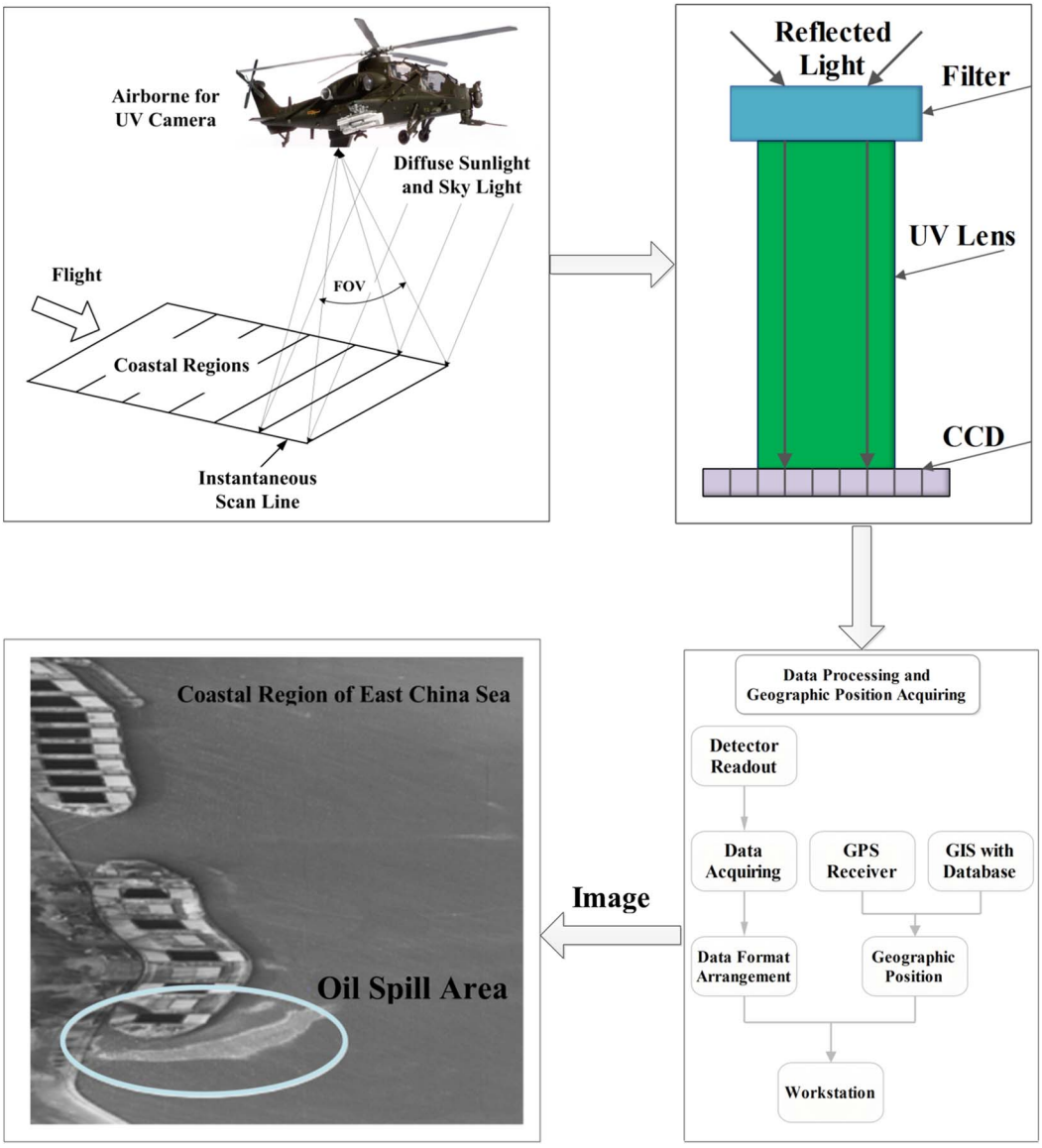

Fig. 5. General flow chart for mapping the oil slick regions using the ultraviolet push-broom imaging system.

B. Imaging Concept

An ultraviolet imaging system concept was designed and its imaging process is shown in Fig. 5. The camera is a "push-broom" imaging system which draws an oil film image as the aircraft flies over oil-covered coastal areas. Light is reflected by the oil-covered sea surface and filtered by the near ultraviolet filter in front of the system. The reflected light enters the designed ultraviolet lens and is received by a linear charge-coupled device (CCD) array. The CCD reads the reflected, filtered light periodically at a rate proportional to the aircraft's ground speed and yields a sequence of one-dimensional data frames. The results of the oil slick data, the global position system (GPS) information, and the geographical information system (GIS) data are transferred to the workstation after each image swath is collected. Images of oil slicks, GPS information, and GIS data in coastal areas were achieved by this ultraviolet push-broom imaging system and urgent action would be taken to curb the rapid expansion of the oil slicks in oil-polluted areas.

3. OPTICAL DESIGN AND OPTOMECHANICAL MODEL

A. Signal-to-Noise Ratio

High spatial resolution and temporal resolution in oil slick surveillance are necessary to acquire the oil-covered regions imagery in a timely and precise manor. Considering the previously stated requirements in Section 1, it is obvious that the FOV of the system must be wide enough to cover relevant oil-covered regions during every flight. To minimize the total axial length and weight of the ultraviolet imaging system and achieve the optical characteristics like the ground sample distance (GSD), the effective focal length is set to 34 mm. On the other hand, the higher SNR must also be considered, as it enables the ultraviolet system to distinguish oil slicks from the surrounding water. The SNR is determined by many parameters such as the quantum efficiency of the CCD, the transmittance of the lens and optical filters, the atmosphere transmittance, and the collection

aperture. In order to achieve a higher SNR for the ultraviolet imaging system with bandwidth ranges from 0.32 to 0.38 μm, antireflection coatings technology for the optical elements are necessary, as this technology can improve the transmittance of this optical system [25]. A bandpass filter UV-2 with a minimum transmittance of 50% from 0.32 to 0.38 μm made by the Guoguang Corporation was chosen in this imaging system to hinder the extra light, except for the near ultraviolet channel entering the optical system, which can reduce stray light entering the ultraviolet imaging system. As is shown in Fig. 6(a) [26], the optical filter is located in front of the designed lens to reduce the stray light. A back-thinned linear CCD image sensor [Fig. 6(b)] [27] was made for line scan cameras by the Hamamatsu Corporation in May of 2014. It has a single pixel size of 24 × 24 μm and is available in pixel formats of 1024 × 4 pixels. These characteristics, such as high spectral response, low readout noise, and low dark current in the ultraviolet channel, make it possible to acquire oil slick images by airborne ultraviolet imaging systems.

The SNR [28] is defined as the ratio of signal power to noise power. The general equation for the SNR is

$$\mathrm{SNR} = \frac{S_e}{N_e} = \frac{S_e}{\sqrt{S_e + \sigma_R^2 + D_e}}, \tag{3}$$

where S_e is number of signal electrons, N_e is number of noise electrons, σ_R is the readout noise ($\sigma_R = 100$ e$^-$rms), and D_e is the dark current ($D_e = 1000$ e$^-$/pixel/s).

The number of signal electrons within the integrated period is expressed as the following equation:

$$S_e = \frac{\pi A_d t_{\mathrm{int}}}{4F^2 h\nu} \int_\lambda L_\lambda \tau_a(\lambda)\tau_0(\lambda)\eta(\lambda)\mathrm{d}\lambda, \tag{4}$$

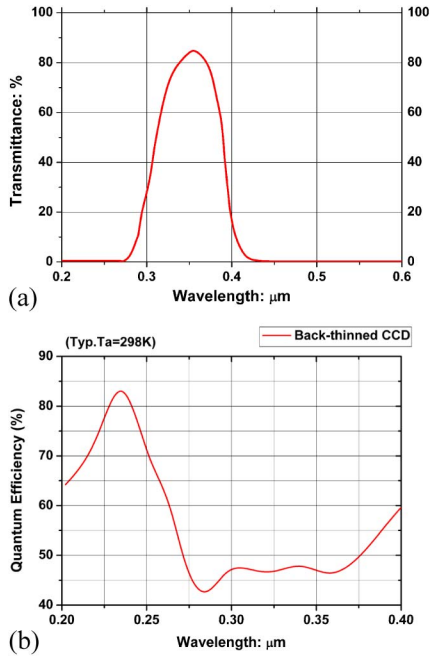

Fig. 6. (a) Transmission spectrum of the UV-2 filters as a function of wavelength. (b) Quantum efficiency of the back-thinned CCD S9037-1002 at 25°C.

where A_d is area of a single pixel, t_{int} is the integration time, F is the F-number, h is Planck's constant, ν is the frequency, L_λ is the equivalent input spectral radiance, $\tau_a(\lambda)$ is the transmittance of the atmosphere, $\tau_0(\lambda)$ is the transmittance of the optical lens, and $\eta(\lambda)$ is the quantum efficiency.

To simplify calculation of the SNR, Eq. (4) can be expressed as

$$S_e = \frac{\pi A_d t_{\mathrm{int}}}{4F^2 h\nu} L_0 \tau_0 \eta_0, \tag{5}$$

where $L_0 = L\Delta\lambda\tau_\alpha$ is the integrated total radiance at the entrance pupil. In this paper, to simplify the calculation of the SNR, τ_α, τ_0, and η_0 are the minimum transmittance of the atmosphere, the minimum transmittance of the optical-camera-included optical filter, and the minimum quantum efficiency, respectively. The specific portion values used to calculate the SNR are listed as below: $t_{\mathrm{int}} = 0.015$ s, $\tau_0 = 0.5$, $\eta_0 = 0.45$, $A_d = 24$ μm × 24 μm. Based on Eqs. (3) and (5), the integrated total radiance L_0, and the specific values listed above, the SNR was calculated and is summarized in Table 1 in Section 3.B.

B. Design Specifications and Description

According to certain concerns stated in Sections 1 and 3.A, the design specifications of previous sensors and this sensor are summarized in Table 1. The comparison shows that this present design summarized in Table 1 provides an improvement in the FOV and a much higher SNR than the ultraviolet line scanner, while the new-style push broom ultraviolet camera provides a narrow FOV. The GSD of the system varies from 0.35 to 0.7 m with flight height ranges from 0.5 to 1 km, which can meet the demands for oil slick surveillance. This ultraviolet imaging system designed by ZEMAX optical software [29] comprises seven elements, as shown in Fig. 7. This is an f/3.4 optical system with an effective focal length of 34 mm and with a less than 10.7 μm spot size across the entire image plane for a ±20 deg FOV. As is shown in Fig. 7, this camera was designed around a common optical axis for easy fabrication and alignment. The separations between different elements are designed to provide adequate mechanical clearances for baffles

Table 1. Comparison of Specifications

	Present Design	Ultraviolet Line Scanner Aboard the HU-25A Aircraft [9]	New-Style Push-Broom Ultraviolet Camera [12,13]
Spectral range (μm)	0.32–0.38	0.32–0.4	0.3–0.37
Cross track FOV (deg)	40	Not stated	15
F-number	3.4	Not stated	2.1
Effective focal length (mm)	34	Not stated	100
Detector angular resolution (mrad)	0.7	5	0.5
SNR	380 (a clear sky case)	17 dB	≥1000

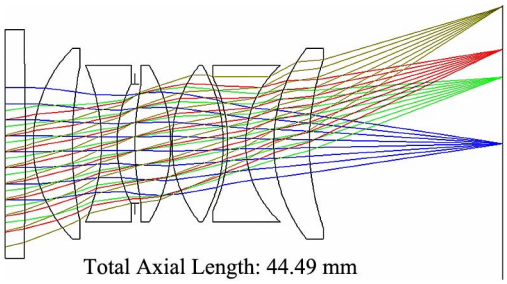

Fig. 7. Optical layout of the ultraviolet lens.

and to balance the comatic and astigmatic aberrations of the system. Surfaces of the seven elements are spherical and the total axial length of this optical layout is about 45 mm. Materials of the optical elements are fused silicon and calcium fluoride (CaF_2).

The modulation transfer function (MTF) represents the image performance of an imaging system, and we propose the MTF response of the designed lens at a wavelength of 0.35 μm in Fig. 8(a). The MTF at the full FOV exceeds 0.60 when the corresponding spatial frequency is 22 lp/mm. The ratio of the image achieved by this ultraviolet imaging system contrast to oil slick areas contrast is higher, and the pollution area is identified and detected better. The relative illumination (RI) is applied to evaluate the brightness over a 40° FOV. If the relative illumination of different FOV is identical, the brightness of the imagery over the full FOV shows no difference for a region polluted by oil uniformly, which would make it distinguish

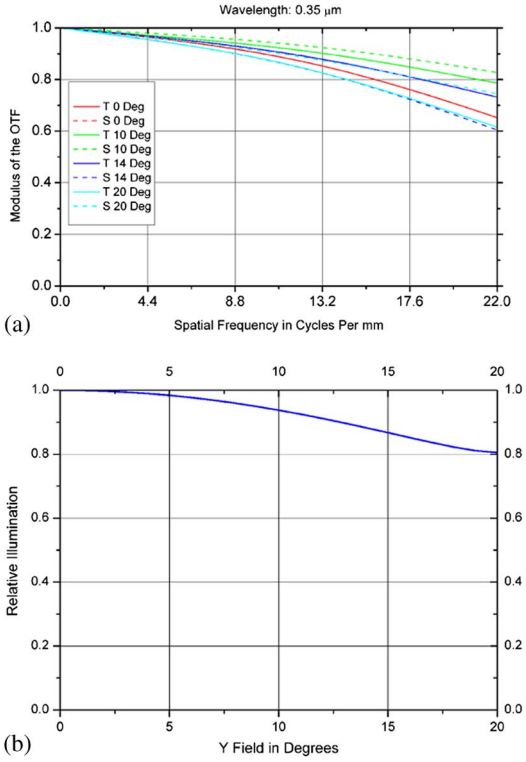

Fig. 8. MTF and RI of the designed ultraviolet lens. (a) MTF versus spatial frequency (T, tangential direction; S, sagittal direction; Deg, degree). (b) RI as a function of different FOV.

oil slicks from the background easily and decrease the influence of misidentification. That is to make the illumination of different FOV as uniform as possible. However, it is clear that keeping uniform illumination over a full FOV is very difficult. The performance of relative illumination of the system is shown in Fig. 8(b). It is clear that the RI is nearly equal to 0.80 at its maximum FOV. Generally speaking, how to balance the MTF and RI during the optical design process is a dilemma. The higher the RI is, the more harmful rays pass through the edge of the image. These harmful rays degrade the systematic MTF seriously, especially for the edge FOV and high spatial frequencies. In this design, we achieved a balance between the RI performance and the MTF performance, especially for the marginal field. Figure 9 is the spot diagram of the whole semi-FOV of this lens. The maximum root mean square (RMS) diameter is about one single pixel size (24 μm) over a full FOV.

The optical distortion is a shape-dependent aberration. The shape and bending factors of the lens are commonly applied to balance the optical distortion at a low level, as shown in Fig. 10 (right). The distortion of the design is controlled in the ranges from 0% to 0.25%. Furthermore, the field curvature (Fig. 10, left) is relative to the Petzval sum. Basically, to reduce the Petzval sum, a lens with high refractive index material should be separated. Also, lens separation reduces spherical aberration. The field curvature of this lens is difficult to correct because the refractive index of fused silicon and CaF_2 shows little difference at the same time the FOV is relatively wider. The maximal value of field curvature is about 0.3 mm. In short, all aberrations are well controlled for this designed lens [30].

C. Performance Modeling

The mechanical configuration of the imaging system was developed to check for any potential fabrication and integration problems prior to fabrication. Figure 11 shows a perspective view of this model of the system. The proposed model has a miniature structure with a total length of 59.1 mm and 65.4 g weight. Thus, it is appropriate as an appliance of this ultraviolet imaging system on the airborne platform. A tolerance analysis

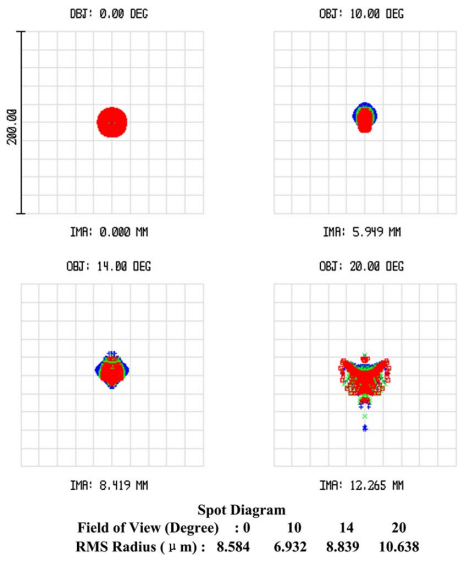

Fig. 9. Spot diagrams through different FOV.

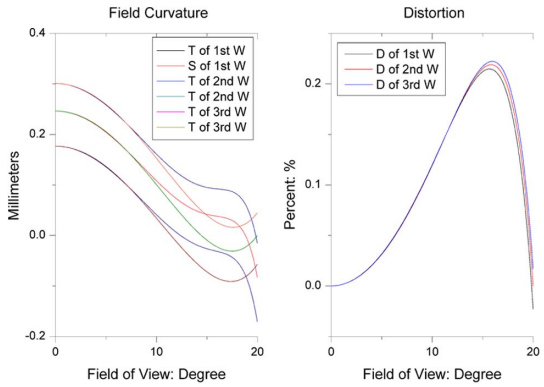

Fig. 10. Field curvatures and distortions of different wavelengths (T, tangential direction; S, sagittal direction; W, wavelength).

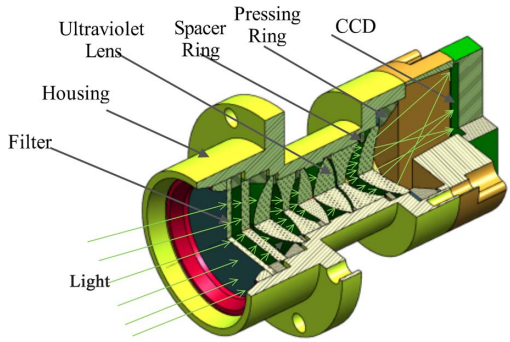

Fig. 11. Three-dimensional solid model of the ultraviolet imaging system.

was performed to check the ability of fabrication. If the moderate tolerances for the surface sag, tilts, decenters, and axial spacing for the ultraviolet system are 20 μm in general, the sensitivity analysis results showed that the estimated average MTF exceeds 0.34 over the full FOV. The results of this tolerance analysis showed that the system performance can be achieved easily with moderate tolerances for the fabrication and assembly. As a result of the moderate tolerance requirements and smaller number of parts, the cost of this ultraviolet camera will be much lower than the cost of a conventional ultraviolet camera.

4. FUTURE PLAN

This ultraviolet imaging camera will be applied for the detection/surveillance of oil slick pollution. The proposed efforts in the future follow a typical development flow: sensor design and manufacturing, performance testing, environmental testing, calibration, data capture, and flight testing. The optomechanical assembly is implemented as soon as the ultraviolet lens and mechanical elements are manufactured. Performance testing is applied to verify its design specifications, and environmental testing is also applied to verify its mechanical properties at external extreme climates. Signal and noise measurements are performed at the specified reference radiance. An accurate wavelength calibration is essential for the retrieval of oil-covered surface reflectance. The ultraviolet imaging system flight testing is planned for autumn 2016, and the corresponding oil slick data are obtained to evaluate the polluted coastal areas. For a specific application, detailed consideration of the ultraviolet system will be implemented and evaluated in the future to meet the demands of oil slick monitoring appliances.

5. CONCLUSIONS

A passive airborne ultraviolet imaging system with a wide FOV and a relatively high SNR, together with oil–seawater contrast, a system concept, calculation of the SNR, comparison of specifications, an optical design, and an optomechanical model were illustrated. The oil above the sea surface can be detected due to a large oil–seawater contrast in a certain wavelength region, especially for the near ultraviolet region, which is major evidence for oil slick surveillance. Furthermore, the oil-covered coastal areas can be assessed better by the near ultraviolet remote sensor than other optical remote sensors. Also, the ultraviolet imaging system can distinguish the dark coastline from the oil-covered sea surface in coastal regions.

High imaging quality of a wide 40° FOV optical system is difficult to achieve because the high-order aberration increases greatly with the growth of the FOV. The MTF of this ultraviolet system exceeds 0.6 when the spatial frequency is 22 lp/mm and the spot diagram diameter is prior to a single pixel size. The GSD of the system varies from 0.35 to 0.7 m with flight height ranges from 0.5 to 1 km, which can meet the demands for oil slick surveillance. In order to reduce the influence of sun glint and nonuniform sky radiance, the viewing geometry of the ultraviolet imaging system aboard the airborne platform is also considered. The model of integrated total radiance by MODTRAN software determines the SNR of the ultraviolet imaging system, and the SNR is 380 for a clear sky case. The miniature structure of the optomechanical model with a total length of 59.1 mm and a weight of 65.4 g make installation possible on the small size airborne system, and the tolerance analysis results showed that the system performance can be achieved easily for the fabrication and assembly.

Funding. National Natural Science Foundation of China (NSFC) (41175028); Science and Technology Project of Changchun (14KG024).

REFERENCES

1. C. E. Brown, M. F. Fingas, M. Fruhwirth, and R. Lloyd Gamble, "Oil spill remote sensing: a brief review of airborne and satellite sensors," in *The SPOT Image 1995 User Group Meeting*, Washington, DC, 1995.
2. C. Brekke and A. H. S. Solberg, "Oil spill detection by satellite remote sensing," Remote Sens. Environ. **95**, 1–13 (2005).
3. M. Gade, J. Scholz, and C. von Viebahn, "On the detectability of marine oil pollution in European marginal waters by means of ERS SAR imagery," IEEE Geosci. Remote Sens. Symp. **6**, 2510–2512 (2000).
4. O. Zielinski, T. Hengstermann, and N. Robbe, "Detection of oil spills by airborne sensors," in *Marine Surface Films* (Springer, 2006), pp. 255–271.
5. M. N. Jha, J. Levy, and Y. Gao, "Advances in remote sensing for oil spill disaster management: state-of-the-art sensors technology for oil spill surveillance," Sensors **8**, 236–255 (2008).

6. P. Wagner, T. Hengstermann, and O. Zielinski, *MEDUSA: An Airborne Multispectral Oil Spill Detection and Characterization System* (International Society for Optics and Photonics, 2000), pp. 610–620.
7. C. E. Catoe and F. L. Orthlieb, "Remote sensing of oil spills," in *International Oil Spill Conference*, Washington, DC, June, 1971, pp. 71–84.
8. F. Carnesecchi, V. Byfield, P. Cipollini, G. Corsini, and M. Diani, "An optical model for the interpretation of remotely sensed multispectral images of oil spill," Proc. SPIE **7105**, 4–12 (2008).
9. J. R. White and R. E. Schmidt, "United States coast guard progress in oil spill surveillance," in *International Oil Spill Conference*, San Antonio, Texas, 1983, pp. 339–344.
10. K. Grüner, R. Reuter, and H. Smid, "A new sensor system for airborne measurements of maritime pollution and of hydrographic parameters," Geojournal **24**, 103–117 (1991).
11. L. Backlund and L. Holmström, "Second generation oil spill and maritime surveillance systems now operational in Sweden," in *International Oil Spill Conference*, San Antonio, Texas, 1983, pp. 349–353.
12. D. Yin, X. Huang, W. Qiao, and X. Huang, "Airborne validation of a new-style ultraviolet push-broom camera for ocean oil spill pollution surveillance," Proc. SPIE **7825**, 1–11 (2010).
13. D. Y. Yin, X. Feng, Y. Zhang, X. Y. Li, X. X. Huang, B. L. Liu, and Q. Feng, "Research of new-style ultraviolet push-broom imaging technology," Proc. SPIE **73840**, 738403 (2009).
14. Z. Otremba, J. Piskozub, and T. Krol, "Modeling the reflectance of sea areas polluted with oil emulsion," Fresenius Environ. Bull. **9**, 1109–1113 (2003).
15. Z. Otremba and J. Piskozub, "Modeling the remotely sensed optical contrast caused by oil suspended in the sea water column," Opt. Express **11**, 2–6 (2003).
16. Q. Tong, B. Zhang, and L. Zheng, *Hyperspectral Remote Sensing* (Higher Education, 2006) (in Chinese).
17. Y. Li, Q. Wang, H. Lv, J. Huang, and Y. Wei, *Water Optical Properties and Ocean Color Remote Sensing of the Taihu Lake* (Science, 2010) (in Chinese).
18. X. Jianwei, "Study on radiative transfer mode and the remote sensing estimation of offshore oil Thickness information," Ph.D. thesis (University of Nanjing, 2011) (in Chinese).
19. Y. Xu, R. Wang, and S. Liu, "Atmospheric correction of hyper spectral data using MOETRAN model," Proc. SPIE **7123**, 1–7 (2008).
20. S. Fang, X. Huang, D. Yin, C. Xu, X. Feng, and Q. Feng, "Research on the ultraviolet reflectivity characteristic of simulative targets of oil spill on the ocean," Spectrosc. Spectral Anal. **30**, 738–742 (2010) (in Chinese).
21. Z. Otremba, "The impact on the reflectance in VIS of a type of crude oil film floating on the water surface," Opt. Express **7**, 129–134 (2000).
22. J. Tang, "The simulation of marine optical properties and color sensing models," Ph.D. thesis (Institute of Remote Sensing and Digital Earth, Chinese Academy of Sciences, 1999) (in Chinese).
23. C. D. Mobley, "Estimation of the remote-sensing reflectance from above-surface measurements," Appl. Opt. **38**, 7442–7455 (1999).
24. A. Berk, L. S. Bernstein, and D. C. Robertson, "MODTRAN: a moderate resolution model for LOWTRAN," Technical Report (Spectral Sciences, 1987).
25. Guoguang Corporation, "Datasheet of standard band-pass filters," http://gggxb1.com/default.asp.
26. E. C. Fest, *Stray Light Analysis and Control* (SPIE, 2013).
27. High-speed operation, back-thinned FFT-CCD. Hamamatsu Photonics K.K. (2014).
28. M. Xu, Q. Feng, and J. Wei, "The calculation of SNR in SWIR detector system for applications to remote sensing system," Infrared Technol. **10**, 588–590 (2006).
29. ZEMAX optical design program, user's guide (2009).
30. D. Malacara-Hernández and Z. Malacara-Hernández, *Handbook of Optical Design* (CRC Press, 2004).